

Axonal Heparan Sulfate Proteoglycans Regulate the Distribution and Efficiency of the Repellent Slit during Midline Axon Guidance

Karl G. Johnson,¹ Aurnab Ghose,¹
Elizabeth Epstein,² John Lincecum,³
Michael B. O'Connor,² and David Van Vactor^{1,*}

¹Harvard Medical School
Department of Cell Biology
Program in Neuroscience
240 Longwood Avenue
Boston, Massachusetts 02115

²Howard Hughes Medical Institute
University of Minnesota
Minneapolis, Minnesota 55455

³Biogen
14 Cambridge Center
Cambridge, Massachusetts 02142

Summary

The presentation of secreted axon guidance factors plays a major role in shaping central nervous system (CNS) connectivity [1]. Recent work suggests that heparan sulfate (HS) regulates guidance factor activity; however, the *in vivo* axon guidance roles of its carrier proteins (heparan sulfate proteoglycans, or HSPGs) are largely unknown [2–4]. Here we demonstrate through genetic analysis *in vivo* that the HSPG Syndecan (Sdc) is critical for the fidelity of Slit repellent signaling at the midline of the *Drosophila* CNS, consistent with the localization of Sdc to CNS axons. *sdc* mutants exhibit consistent defects in midline axon guidance, plus potent and specific genetic interactions supporting a model in which HSPGs improve the efficiency of Slit localization and/or signaling. To test this hypothesis, we show that Slit distribution is altered in *sdc* mutants and that Slit and its receptor bind to Sdc. However, when we compare the function of the transmembrane Sdc to a different class of HSPG that localizes to CNS axons (Dallylike), we find functional redundancy, suggesting that these proteoglycans act as spatially specific carriers of common HS structures that enable growth cones to interact with and perceive Slit as it diffuses away from its source at the CNS midline.

Results and Discussion

The midline of the CNS has been a powerful model system for studies of growth cone navigation. These studies have revealed that a common logic of axon guidance mechanisms has been well conserved from invertebrate to mammalian species (reviewed in [1]). At the midline, specialized glial cells release long-range attractive and repellent cues to direct the passage of axons from one side of the nervous system to the other. The decision to cross the midline is controlled in many organisms by the secreted repellent factor Slit and its

axonal receptors in the Roundabout (Robo) family. Slit appears to act at a distance to regulate midline crossing behavior and to define the lateral positioning of axon tracts within the neuropil (reviewed in [5]). However, the mechanisms that shape the putative gradient of Slit protein, and the response of Robo-expressing growth cones to Slit, are under intensive study. Given our interest in understanding these mechanisms in detail, we were intrigued by the observation that the efficiency of guidance responses to Slit depends on the carbohydrate polymer heparan sulfate (HS) [6]. HS is a highly charged polysaccharide found on several types of HS proteoglycans (HSPGs) (reviewed in [2]). Although HS biosynthesis has been recently shown to be important for midline axon guidance *in vivo* [7], the guidance roles of its carrier proteins are unknown.

The majority of cell surface HS polymers are carried by two classes of HSPGs: the transmembrane Syndecans and the glycosylphosphatidylinositol (GPI)-linked Glypicans (reviewed in [2]). While mammalian species express a number of genes in each of these classes, *Drosophila* has one Syndecan gene (*sdc*) and two Glypican genes (*dally* and *dallylike*). Although some degree of core-protein specificity has been observed in functional comparisons between different HSPGs during early pattern formation and cell fate determination (reviewed in [8]), true loss-of-function mutations have yet to be analyzed for *sdc* and *dallylike* (*dlp*). Although anti-Sdc antibodies had been previously described [9], we developed methods to image Sdc protein at improved resolution and showed that the antibody recognizes Sdc (Figure S1) and that Sdc localizes to both longitudinal and commissural axons pathways within the *Drosophila* embryonic CNS (Figure 1A). Our finding that Sdc localization overlaps heavily with Robo receptor expression made Sdc an excellent candidate for further analysis (Figure 1A).

The availability of two P-element insertions (*P10608* and *KG06163*) into the *sdc* locus made it possible for us to address *sdc* function by making a small excision-induced deletion [*Df(2R)48*] removing the first two exons of *sdc*, including the promoter and 5' untranslated region, the translational start codon, and the signal sequence (Figure S2). To confirm the prediction that this deletion eliminates Sdc protein expression, we stained *Df(2R)48* embryos with an antibody that recognizes the extracellular domain near the transmembrane region of Sdc [9]. We found only a minute residual signal that may represent either nonspecific background or limited perdurance of maternally loaded Sdc (Figure 1A). Importantly, simultaneous staining of these mutants with anti-Robo antibodies revealed that although levels of Robo expression appeared normal in *Df(2R)48*, Robo-positive axons now crossed the CNS midline where Slit concentration is normally at its highest (Figure 1A). We also found that ventral muscles overshoot their insertion sites in strong *sdc* mutants (data not shown), reminiscent of defects in *slit* mutants [10]. To be certain that perturbation of the neighboring genes *sara* and *FKB13*

*Correspondence: davie@hms.harvard.edu

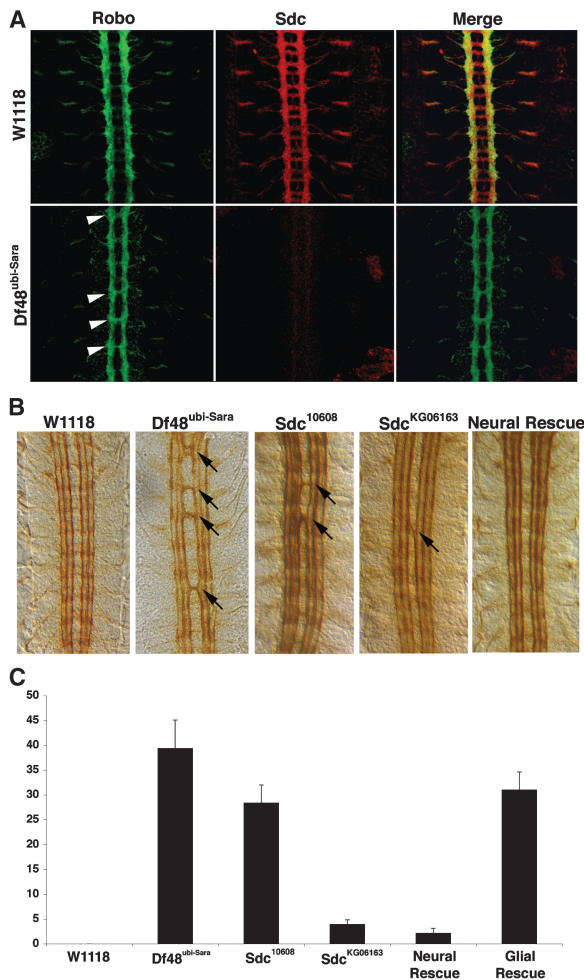


Figure 1. Syndecan Is Required for Accurate Midline Guidance

(A) Using antibodies to Robo and Sdc allowed detection of high levels of expression of both proteins on longitudinal fascicles, on motor axons, and at muscle insertions sites in stage 16 embryos. Sdc is also expressed on commissural fascicles, and with this as the only exception, Sdc and Robo show a high degree of coexpression. *Df48^{ubi-sara}* mutants have dramatic reductions in Sdc expression, and Robo-positive fascicles can be seen crossing the CNS midline in these mutants (arrowheads).

(B) Anti-Fas II staining of stage 17 embryos show a high frequency of midline-crossing defects (arrows) in both *Df48^{ubi-sara}* and *sdc¹⁰⁶⁰⁸* homozygous mutants, and infrequent midline crossing is observed in *sdc^{KG06163}* mutants. Neural expression of a *sdc* transgene (*elav-Gal4* x *UAS-sdc*) eliminates 90% of the midline-crossing defects observed in homozygous *Df48^{ubi-sara}* embryos.

(C) Quantification of segments exhibiting abnormal crossing of FasII-positive fascicles in *w¹¹¹⁸*, *Df48^{ubi-sara}/Df48^{ubi-sara}*, *sdc¹⁰⁶⁰⁸/sdc¹⁰⁶⁰⁸*, *sdc^{KG06163}/sdc^{KG06163}*, *Df48^{ubi-sara}/Df48^{ubi-sara}*, *elav-Gal4/UAS-sdc* and *Df48^{ubi-sara}/Df48^{ubi-sara}; slit-GAL4/UAS-sdc* ($n = 407, 325, 433, 331, 470$, and 385 segments, respectively).

was not responsible for the guidance errors, we examined mutations in each locus (data not shown) and also introduced a *sara* rescue construct into the *Df(2R)48* background (Figure 1, see Experimental Procedures). We found that these flanking genes do not contribute to the midline phenotype of *Df(2R)48*. Because HS is known to facilitate cell fate decisions in other contexts, we also examined both neuronal and midline glial pat-

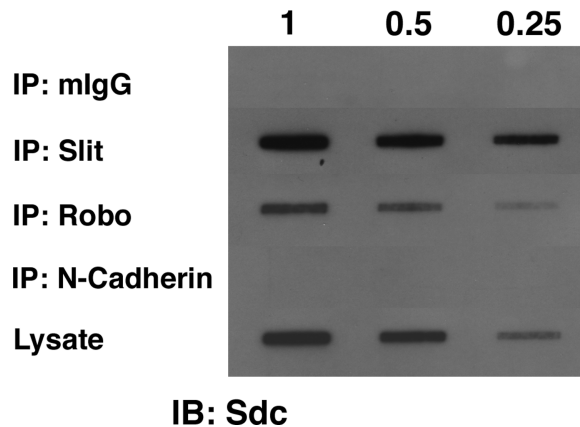


Figure 2. Endogenous Slit and Robo Bind to Syndecan

Using *Drosophila* cell extracts, we performed immunoprecipitations (IP) with nonspecific murine IgG antibodies (mlgG), anti-Slit monoclonal antibodies ascites (Slit), anti-Robo monoclonal supernatant (Robo), and anti-N-Cadherin affinity-purified polyclonal antisera (N-Cadherin) (see the Experimental Procedures). Three dilutions of each precipitate, and dilutions of the input extract, were blotted to membrane and probed with affinity-purified anti-Sdc. Although both Slit and Robo IPs detect a strong Sdc signal compared to input controls, we find no Sdc signal in the negative controls (mlgG and N-Cadherin).

terning but found no defects (Figure S3). Moreover, levels of Slit expression in midline glia appeared to be comparable to wild-type levels.

To quantify the midline guidance defects in different *sdc* alleles, we used mAb 1D4 to visualize ipsilateral axon fascicles and scored the frequency of ectopic midline crossing (Figures 1B and 1C). We found an allelic series of phenotypic penetrance ranging from 5%–40%, suggesting that the efficiency of axon guidance depends on the amount of Sdc present. However, because Sdc family members are known to be proteolytically processed and released from the cell surface [2], it was important to determine whether Sdc functions autonomously to axons. We used a *sdc* cDNA under the control of the GAL4 upstream activating sequence and compared its ability to rescue the *Df(2R)48* phenotype under the control of either a midline glial-specific GAL4 source (*slit-GAL4*) or a postmitotic neuron-specific source (*elav-GAL4*). Only neuronal expression of Sdc rescues the guidance errors (Figure 1C), suggesting that Sdc acts locally to increase growth cone sensitivity to Slit.

Because *sdc* axon phenotypes suggest the Slit signaling system's failure to restrict midline crossing, we asked if *sdc* mutations display specific genetic interactions with mutations in *slit* or its receptors. Using the same assay that identified Slit as the Robo ligand [10], we compared embryos transheterozygous for *sdc* and mutations in several loci (Figure S4). We find highly significant ($p < 0.005$) interactions between *sdc* and both *slit* and *robo* in this assay. This interaction appears to be specific because no enhancement is observed when *sdc* is combined with a mutation in the receptor tyrosine phosphatase gene *DPTP69D*, which is known to contribute to midline guidance [11]. Although no interaction is seen between *sdc* and single mutations in *robo2* or

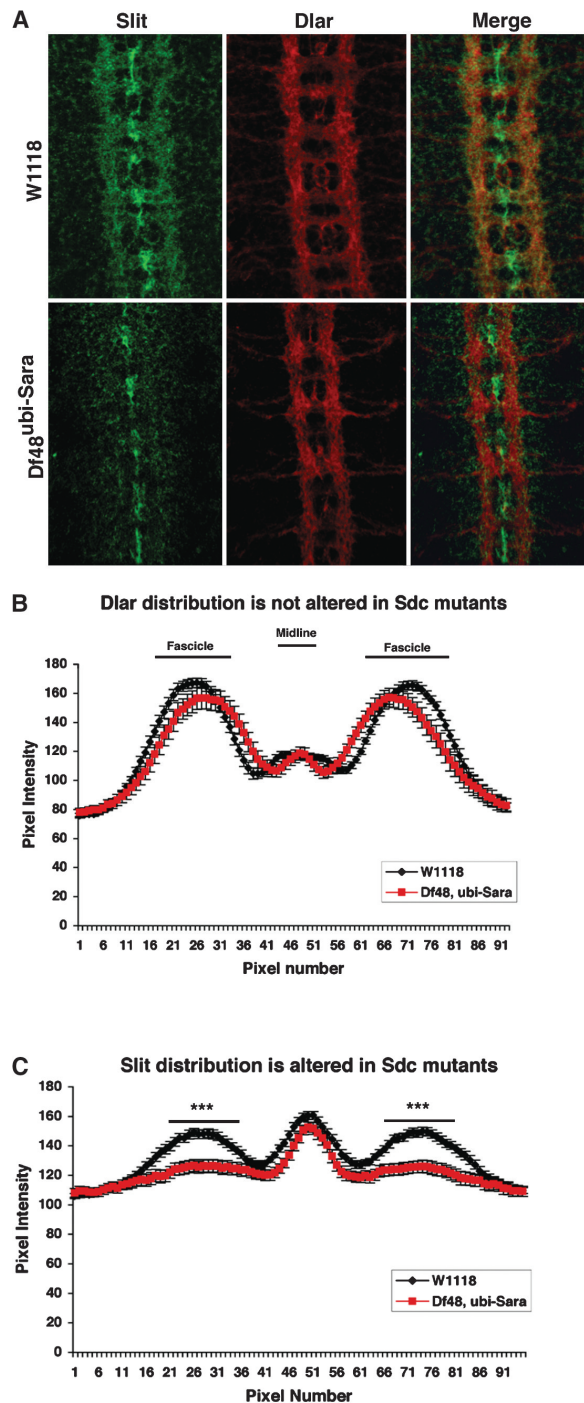


Figure 3. Slit Distribution Is Abnormal in *syndecan* Mutants
 (A) z projections of the central nervous systems of wild-type and *sdc* mutant stage 15 embryos stained for cell-surface Slit and Dlar. *Sdc* mutants have subtle qualitative differences in both Slit and Dlar protein distribution. In *Sdc* mutants, there appears to be a reduction in the amount of Slit protein on longitudinal fascicles, whereas Dlar immunostaining suggests that the longitudinal fascicles have shifted closer to the midline.
 (B) Quantitative analysis of Dlar distribution in wild-type and *sdc* mutant stage 15 embryos. No significant differences were detected in Dlar protein distribution, although a trend toward a medial shift in fascicle position was observed in *sdc* mutants.

robo3, crosses between *sdc* and double mutants removing *robo* and one of the other *robo* family genes (e.g., *robo*, *robo2*) reveal significant increases in the interaction when they are compared to *robo* alone (Figure S4). These genetic results suggest that Sdc acts in the Slit-Robo pathway.

Genetic assays provide a sensitive means of detecting an in vivo interaction between different components in a pathway, but they do not show that the association is direct. Thus, we developed a biochemical assay to determine whether Sdc binds to Slit and/or Robo in cellular extracts in which all three proteins are endogenously expressed (see the Experimental Procedures). Immunoprecipitation of either Slit or Robo and subsequent detection with anti-Sdc antibodies reveals that Sdc associates with both Slit and its receptor (Figure 2), suggesting the possibility of a ternary complex. This association is specific because no Sdc is trapped by nonspecific IgG or N-Cadherin antibodies that successfully IP other signaling molecules (Figure 2). Thus, Sdc participates directly in a complex with Slit and Robo.

Having gathered multiple lines of evidence revealing a role for Sdc in Slit signaling, we were now in a position to test popular models for the underlying mechanism. HS has been proposed to support the patterning activity of several secreted ligands by restricting their diffusion from a focal source (e.g., [12–14]). If this were the case for Sdc in Slit signaling, we would predict a change in the distribution of Slit at sites distant from the midline glia. To examine this, we optimized an immunohistochemical method to allow visualization of Slit protein not only on the surface of midline glia but also within the CNS neuropil (Figure 3A). We found no gross qualitative difference in the pattern of Slit distribution between *Df(2R)48* and wild-type controls. However, rigorous quantitative analysis of confocal images with an independent axon surface marker (LAR) as an internal control to ensure comparable signal strength (Figure 3B) reveals that *sdc* mutants show a highly significant change in the pattern of Slit accumulation throughout the neuropil (Figure 3C, see legend for statistics). Slit is still highly expressed on midline glia in *sdc* mutants, but the Slit signal is significantly reduced in the neuropil. These data are highly reproducible (three experiments showed nearly identical results) and are consistent with the ligand-trapping model anticipated from previous studies on HS.

The striking difference in protein structure between Syndecans and Glypicans raises two related questions: (1) is there core-protein specificity to HSPG function on the growth cone surface, or are these proteins acting mainly as carriers for a common HS structure? and (2) are the cytoplasmic domains of Sdc, known to interact with signaling proteins inside the cell (e.g., [15]), essen-

(C) Quantitative analysis of Slit distribution by the same method described in (B). Although there is no significant difference in the level of Slit in the periphery and at the midline, a significant reduction in the amount of slit protein was detected on the longitudinal fascicles in *sdc* mutants (***) indicates $p < 0.005$). Plots shown represent 3000 individual line scans in ten mutant and ten wild-type age-matched embryos.

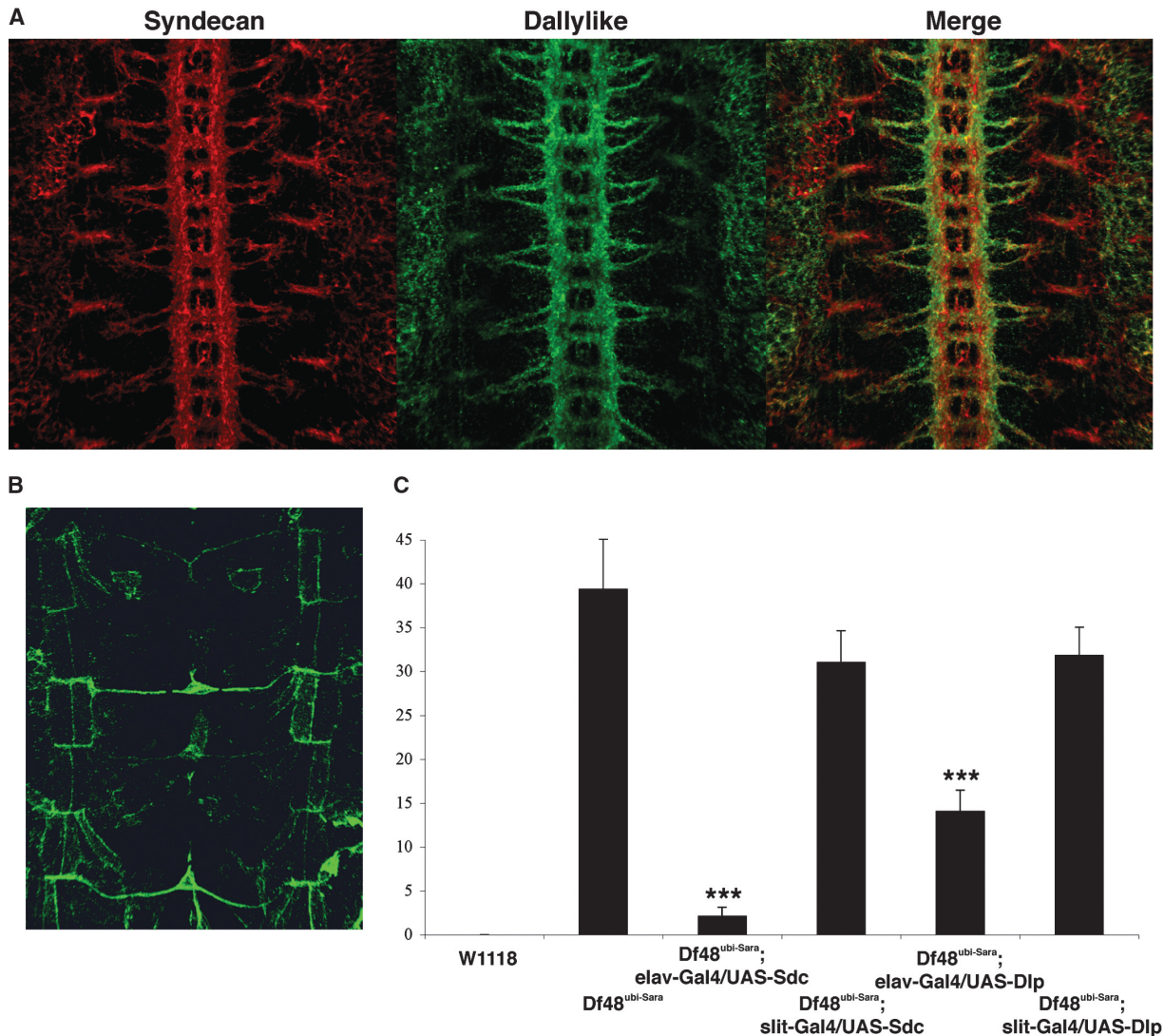


Figure 4. Syndecan and Dallylike Have Overlapping Localization and Function

(A) Syndecan and Dallylike show highly overlapping, yet distinct, patterns of endogenous expression in the developing CNS.

(B) Overexpression of Dallylike by a paired-Gal4 driver shows high levels of Dallylike expression in mesectodermal cells and in muscles 6 and 7; this expression pattern is never observed in a wild-type embryo, demonstrating the specificity of the 13G8 antibody.

(C) Postmitotic neural expression of Syndecan or Dallylike can significantly rescue the midline guidance defects observed in *sdc* mutant embryos ($p < 0.005$), but expression of these constructs in midline glia does not.

tial for Sdc function during axon guidance? We answered both of these questions by testing the specificity of Sdc relative to another HSPG. Of course, it was important to compare Sdc to an HSPG normally localized to axons if possible. Using an existing antibody [16], we were able to show that Glypican Dallylike (Dlp) is expressed on the surface of embryonic axons in a pattern nearly identical to that of Sdc (Figure 4A). This antibody recognizes Dlp ectopically expressed by a *UAS-dlp* transgene (Figure 4B) [13]. When *UAS-dlp* was expressed in a *Df(2R)48* background under the control of a *Slit-GAL4* driver, we found no significant rescue of the *sdc* midline phenotype (Figure 4C). However, neuron-specific expression of Dlp generated a highly significant degree of functional rescue ($p < 0.005$). This clearly shows that an increase in Dlp expression can compen-

sate for the loss of Sdc, consistent with the finding that Slit can bind to at least one mammalian Glypican [17]. In addition, this experiment shows that the unique intracellular signaling motifs found in Sdc are not essential for Slit signaling.

In conclusion, we find that Sdc localizes to developing axons, is required for accurate growth cone navigation at the CNS midline, and interacts genetically and physically with Slit and Robo. Although a full account of HSPG functional specificity awaits the analysis of mutations in *dallylike*, the fact that both Syndecan and Glypican can serve interchangeably to improve the efficiency of growth cone repulsion suggests a model in which the total amount of cell surface HS determines the sensitivity of Robo-expressing growth cones to the midline repellent. Of course, we cannot rule out the possibility that

the highly conserved cytoplasmic domains of Sdc play a more subtle modulatory function in this context or an essential function in some distinct context. This might explain the difference in the efficiency of Dlp and Sdc in the rescue of *sdc* guidance defects. These and other answers will come from future dissection of the Sdc mechanism and the action of HSPGs in neural development.

Experimental Procedures

Genetic Stocks

Df(2R)48 was generated by imprecise excision of *sdc*¹⁰⁶⁰⁸. This deficiency was found to uncover Sdc, Sara and FKB13 based on its failure to complement *Sdc*¹⁰⁶⁰⁸, *Sara*, and *FKB13* alleles *SARA*²⁵⁰ and *I(2)00734*. A *ubiquitin-Sara* transgene was recombined onto the *Df(2R)48* (*Df48*^{ubi-Sara}) chromosome because this transgene was shown to be capable of rescuing the Sara loss-of-function phenotype. *Sdc*^{KG06163}, *sdc*¹⁰⁶⁰⁸, *elav-Gal4*, and *slit*² were obtained from the Bloomington Stock Center. *Robo*^{GA285}, *robo3*¹ and *robo*^{GA285}, *robo2*⁸ double mutants were obtained from B. Dickson. All mutations on the second chromosome were balanced over CyO-[actin-lacZ] or CyO-(wingless-lacZ).

Immunohistochemistry

Polyclonal anti-Sdc antisera raised against a fusion protein of glutathione S-transferase with amino acids 165–337 of the extracellular domain of *Drosophila* Sdc was affinity purified as described previously [9]. 1D4 [18] immunohistochemistry was performed as previously described [19], with a 1:5 dilution of the antibody. Anti-Sdc immunostaining worked best on live-dissected stage 14–16 embryos. Embryos were manually dechorionated and filleted along their dorsal surface with tungsten needles. These embryos were immobilized on a microscope slide under PBS, the gut was removed, and the edges of the pelt were pressed to the slide. Pelts were fixed for 20 min in 4% formaldehyde in PBS, washed three times in PBS (or PBS + 0.1% Triton), blocked for 60 min in PBS + 5% heat-inactivated goat serum, and incubated with combinations of the following antibodies: anti-Sdc (1:250) [9], anti-Robo (1:5) [10], anti-Wrapper (1:5) [20], anti-Slit (1:5) [10], anti-Engrailed (1:1) [21], and anti-Dlp 13G8 (1:4) [16]. After extensive washing in PBS, pelts were incubated for 1–2 hr in 1:500 dilutions of goat-anti-mouse Alexa488 or goat-anti-rabbit Alexa568 (both from Molecular Probes). After immunohistochemistry, pelts were washed in PBS and mounted in SlowFade (Molecular Probes).

Immunoprecipitation of Slit and Robo Proteins

Kc167 cells were lysed, and the membrane fraction was separated from the hydrophilic fraction with the Mem-Per membrane protein extraction kit (Pierce). Lysates were precleared for 60 min with GammaBind beads (Amersham) and then incubated overnight at 4°C with beads and monoclonal antibodies against Slit (DSHB), Robo (DSHB), N-Cadherin [22], and mouse IgG (Upstate) as a control. After washes with NP-40 buffer (0.1% NP-40, 150 mM NaCl, 50 mM Tris [pH 7.5]) and PBS, the complexes were eluted with 100 mM glycine (pH 2.5) and immediately neutralized with Tris buffer (pH 9). Three dilutions of the immunoprecipitations (100%, 50%, and 25%) were transferred to Hybond N+ membrane (Amersham) via the slot blot method (Biorad) and analyzed by immunoblotting with the anti-Sdc rabbit polyclonal antibody.

Statistical Analysis of Genetic Interactions

In order to perform statistical analysis on the non-normally distributed data on the frequency of midline crossing events in mutant embryos, we grouped embryos into one of five bins according to the number of midline crossing events observed per embryo. To determine if a particular population of embryos had a significant change in the frequency of midline crossing events, we conducted χ^2 tests with tables comparing the distribution of data into the bins.

Confocal Microscopy

Three-dimensional analysis of antibody staining was conducted on a Nikon E800 microscope and a Bio-Rad Radiance confocal microscope. Optical sections of 0.35 μm were taken across the depth of the filleted embryo and were reassembled with Volocity software from Improvion. Prior to image collection, laser power and gain were decreased in order to prevent saturation of fluorescent signal intensity. Premixing all antibodies minimized subtle changes in antibody concentration between samples. Identical laserpower, gain, and iris settings were used for the collection of data from all embryos. For quantification of the levels of Slit and Dlar protein, 100 μm -long lines were drawn perpendicular to the CNS midline of an image of a z projection. A linescan of pixel intensity along this line was averaged for 100 μm along the anterior-posterior axis. Non-normalized data were plotted according to pixel number, and t tests comparing the pixel intensity at each pixel were conducted.

Supplemental Data

Four supplemental figures are available with this article online at <http://www.current-biology.com/cgi/content/full/14/6/■■■■/DC1/>.

Acknowledgments

We would like to thank Gyeong-Hun Baeg, Norbert Perrimon, and Stefan Thor for *Drosophila* stocks. We thank our colleagues Mark Emerson and Bharatkumar Patel for invaluable assistance and insight. We would also like to thank Jennifer Waters-Schuler at the Nikon Imaging Center at Harvard Medical School for assistance with confocal microscopy and Norbert Perrimon for critical comments on the manuscript. We are very grateful to Dr. T. Uemura for anti-N-Cadherin antibodies. We also thank the Developmental Studies Hybridoma Bank (DSHB) for its repository of available antibodies; the DSHB was developed under the auspices of the National Institute of Child Health and Development and maintained by the University of Iowa, Department of Biological Sciences. D.V.V. is a Leukemia and Lymphoma Society Scholar and is supported by grants from the National Institute of Neurological Disease and Stroke (NS35909 and NS40043). M.B.O. is supported by funds from the Howard Hughes Medical Institute, and K.G. J. is supported by a postdoctoral fellowship from the Helen Hay Whitney foundation.

Received: January 22, 2004

Revised: January 30, 2004

Accepted: January 30, 2004

Published online: February 5, 2004

References

1. Dickson, B.J. (2002). Molecular mechanisms of axon guidance. *Science* 298, 1959–1964.
2. Bernfield, M., Gotte, M., Park, P.W., Reizes, O., Fitzgerald, M.L., Lincecum, J., and Zako, M. (1999). Functions of cell surface heparan sulfate proteoglycans. *Annu. Rev. Biochem.* 68, 729–777.
3. Lander, A.D., and Selleck, S.B. (2000). The elusive functions of proteoglycans: in vivo veritas. *J. Cell Biol.* 148, 227–232.
4. Yamaguchi, Y. (2001). Heparan sulfate proteoglycans in the nervous system: their diverse roles in neurogenesis, axon guidance, and synaptogenesis. *Semin. Cell Dev. Biol.* 12, 99–106.
5. Rusch, J., and Van Vactor, D. (2000). New roundabouts send axons into the Fas lane. *Neuron* 28, 637–640.
6. Hu, H. (2001). Cell-surface heparan sulfate is involved in the repulsive guidance activities of Slit2 protein. *Nat. Neurosci.* 4, 695–701.
7. Inatani, M., Irie, F., Plump, A.S., Tessier-Lavigne, M., and Yamaguchi, Y. (2003). Mammalian brain morphogenesis and midline axon guidance require heparan sulfate. *Science* 302, 1044–1046.
8. Baeg, G.H., and Perrimon, N. (2000). Functional binding of secreted molecules to heparan sulfate proteoglycans in *Drosophila*. *Curr. Opin. Cell Biol.* 12, 575–580.
9. Spring, J., Paine-Saunders, S.E., Hynes, R.O., and Bernfield, M. (1994). *Drosophila* syndecan: conservation of a cell-surface

- heparan sulfate proteoglycan. *Proc. Natl. Acad. Sci. USA* **91**, 3334–3338.
10. Kidd, T., Bland, K.S., and Goodman, C.S. (1999). Slit is the midline repellent for the robo receptor in *Drosophila*. *Cell* **96**, 785–794.
 11. Sun, Q., Bahri, S., Schmid, A., Chia, W., and Zinn, K. (2000). Receptor tyrosine phosphatases regulate axon guidance across the midline of the *Drosophila* embryo. *Development* **127**, 801–812.
 12. Reichsman, F., Smith, L., and Cumberledge, S. (1996). Glycosaminoglycans can modulate extracellular localization of the wingless protein and promote signal transduction. *J. Cell Biol.* **135**, 819–827.
 13. Baeg, G.H., Lin, X., Khare, N., Baumgartner, S., and Perrimon, N. (2001). Heparan sulfate proteoglycans are critical for the organization of the extracellular distribution of Wingless. *Development* **128**, 87–94.
 14. Park, Y., Rangel, C., Reynolds, M.M., Caldwell, M.C., Johns, M., Nayak, M., Welsh, C.J., McDermott, S., and Datt, S. (2003). *Drosophila* perlecan modulates FGF and hedgehog signals to activate neural stem cell division. *Dev. Biol.* **253**, 247–257.
 15. Kinnunen, T., Kaksonen, M., Saarinen, J., Kalkkinen, N., Peng, H.B., and Rauvala, H. (1998b). Cortactin-Src kinase signaling pathway is involved in N-syndecan-dependent neurite outgrowth. *J. Biol. Chem.* **273**, 10702–10708.
 16. Lum, L., Yao, S., Mozer, B., Rovescalli, A., Von Kessler, D., Nirenberg, M., and Beachy, P.A. (2003). Identification of Hedgehog pathway components by RNA in *Drosophila* cultured cells. *Science* **299**, 2039–2045.
 17. Liang, Y., Annan, R.S., Carr, S.A., Popp, S., Mevissen, M., Margolis, R.K., and Margolis, R.U. (1999). Mammalian homologues of the *Drosophila* slit protein are ligands of the heparan sulfate proteoglycan glypican-1 in brain. *J. Biol. Chem.* **274**, 17885–17892.
 18. Van Vactor, D., Sink, H., Fambrough, D., Tsou, R., and Goodman, C.S. (1993). Genes that control neuromuscular specificity in *Drosophila*. *Cell* **73**, 1137–1153.
 19. Van Vactor, D., and Kopczynski, C.C. (1999). Techniques for anatomical analysis of the *Drosophila* embryonic nervous system. In *A Comparative Methods Approach to the Study of Oocytes and Embryos*, J. Richter, Ed. (New York: Oxford University Press), pp. 490–513.
 20. Noordermeer, J.N., Kopczynski, C.C., Fetter, R.D., Bland, K.S., Chen, W.Y., and Goodman, C.S. (1998). Wrapper, a novel member of the Ig superfamily, is expressed by midline glia and is required for them to ensheath commissural axons in *Drosophila*. *Neuron* **21**, 991–1001.
 21. Patel, N.H., Martin-Blanco, E., Coleman, K.G., Poole, S.J., Ellis, M.C., Kornberg, T.B., and Goodman, C.S. (1989). Expression of engrailed proteins in arthropods, annelids, and chordates. *Cell* **58**, 955–968.
 22. Lee, C.H., Herman, T., Clandinin, T.R., Lee, R., and Zipursky, S.L. (2001). N-cadherin regulates target specificity in the *Drosophila* visual system. *Neuron* **30**, 437–450.